ACS OMEGA

http://pubs.acs.org/journal/acsodf

Article

First-Principles Observation of Bonded 2D B_4C_3 Bilayers

Jiacai Shen, Feng Zheng, Shaoxian Wang, Zi-Zhong Zhu, Shunqing Wu, Xiao-Fei Li,* Xinrui Cao,* and Yi Luo

Cite This: *ACS Omega* 2021, 6, 13218−13224

Read Online

ACCESS | Metrics & More | Article Recommendations | Supporting Information

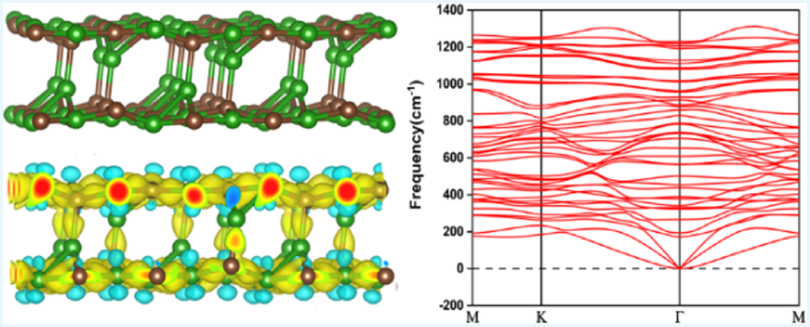

ABSTRACT: Two-dimensional (2D) B−C compounds possess rich allotropic structures with many applications. Obtaining new 2D B_4C_3 structures is highly desirable due to the novel applications of three-dimensional (3D) B_4C_3 in protections. In this work, we proposed a new family of 2D B_4C_3 from the first-principles calculations. Distinct from previous observations, this family of 2D B_4C_3 consists of bonded 2D B_4C_3 bilayers. Six different types of bilayers with distinct bonded structures are found. The phonon spectrum calculations and ab initio molecular dynamics simulations at room temperature demonstrate their dynamic and thermal stabilities. Low formation energies suggest the high possibility of realizing such structures in experiments. Rich electronic structures are found, and the predicted Young's moduli are even higher than those of the previous ones. It is revealed that the unique electronic and mechanical properties are rooted in the bonding structures, indicating the prompting applications of this family of 2D B_4C_3 materials in photovoltaics, nanoelectronics, and nanomechanics.

1. INTRODUCTION

Three-dimensional (3D) B−C compounds have novel properties and applications, especially B_4C_3 in protections.[1,2] For miniaturizations and enhancing performances, lower-dimensional B−C compounds have attracted growing interest recently.[3−7]

Two-dimensional (2D) B−C compounds are rich in configurations due to the diverse bonding patterns of the B and C atoms[6] because boron, known as a deficient atom, tends to form a multicenter bond to share electrons. When it bonds with C to form B−C systems, some peculiar bonding characteristics, such as planar tetracoordinate and pentacoordinate carbons, develop,[4,5,8−12] giving rise to unique physical and chemical properties. For example, B_2C sheets are predicted to be 2D phonon-mediated superconductors with a relatively high transition temperature (T_c) due to the unique planar tetracoordinate bonding manner.[13]

On the basis of the thickness of the reported 2D B−C compounds, they can be classified as monolayer, bilayer, and multilayer 2D B−C. The first synthesized stable and metastable 2D BC_3 honeycomb monolayers were reported by Yanagisawa et al. by an epitaxial method on the NbB_2 surface,[14,15] and the phonon dispersion curves of such materials were obtained.[16] Using the hot filament chemical vapor deposition (HFCVD) method, Jafari et al.[17] also synthesized BC_3 honeycomb sheets. Apart from BC_3, other 2D B−C systems have also been reported in experiments.[18] These successfully fabricated B−C sheets inspired the exploration of new 2D B−C compounds both experimentally and theoretically.

Besides B_2C and BC_3, many new types of stable or metastable 2D B−C systems with various B−C stoichiometric compositions have been reported.[19,20] These boron carbides with finite thicknesses are predicted to be nonmagnetic semiconductors, semimetals, or metals. Among these structures, there are two families of 2D B_4C_3, which are two types of B_4C_3 monolayers[21,22] and one type of a sandwich-like B_4C_3 multilayer.[20] Interestingly, the graphene-like BC monolayer (having a honeycomb structure) is known as a surface-like

Received: February 26, 2021
Accepted: May 4, 2021
Published: May 13, 2021

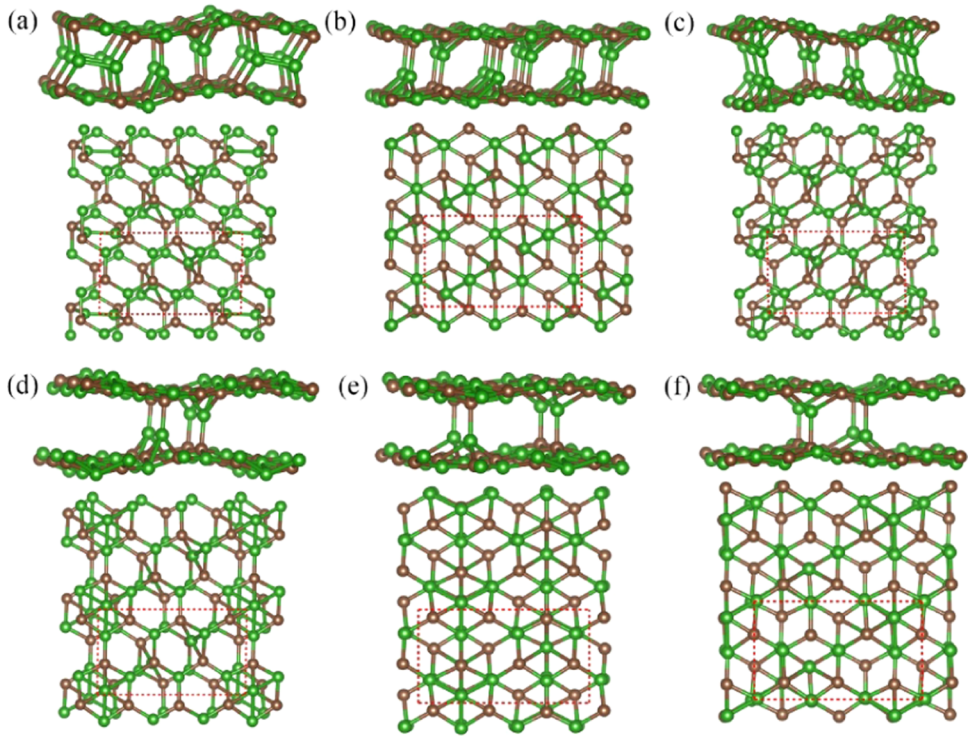

Figure 1. Optimized geometric structures including the side view (upper) and top view (lower) of (a) B_4C_3-I, (b) B_4C_3-II, (c) B_4C_3-III, (d) B_4C_3-IV, (e) B_4C_3-V, and (f) B_4C_3-VI. The red dash depicts the calculated unit cell, and the green and brown balls stand for the B and C atoms, respectively.

layer of 3D B_4C_3 with some atomic reorganizations that happened due to existing dangling bonds. Thus, some unexpected bonding patterns such as planar hexacoordinate B and planar tetracoordinate B/C appear in the interlayer.[20] However, the multilayer is composed of two surface-like monolayers and an interlayer domain that is a bulk-phase-like layer. Hence, it can be considered a triple-layer system, with two surface-like layers and a sandwiched bulk-like layer. The triple layer also contains mixed bonding characters, specifically, sp^2- and sp^3-hybridized B atoms, unconventional tetracoordinate sp^3, and nonplanar hexacoordinate C atoms. It is well known that the bonding nature of bulk-phase B_4C_3 is simple and it only contains a B−C bond. When bulk-phase B_4C_3 changes to low-dimensional B_4C_3, delocalized multicenter bonding patterns occur due to atomic reorganizations, leading to some unexpected planar high-coordinated B/C atoms. Moreover, the B atom can also form B−B bonds in low-dimensional B_4C_3. Combined with the conventional bonding characteristics, the bonding patterns in 2D B_4C_3 are more complex, and the enriched chemical bonding characteristics give rise to the diverse configurations of 2D B_4C_3.

Meanwhile, it is very possible to construct new types of 2D B_4C_3 structures by rational designing. Note that two families of 2D B_4C_3 that are a B_4C_3 monolayer[21,22] and a sandwich-like B_4C_3 triple layer[20] are proposed previously. Logically, we are heavily intrigued to know that whether there exist more 2D B_4C_3 bilayer structures.

In this work, by performing structural designing and first-principles calculations, we report the observation of a new family of 2D B_4C_3 structures, that is, bonded 2D B_4C_3 bilayers. It is revealed that the bonding structures formed in the interface vastly reduced the energy, directly resulting in the formation of bonded 2D B_4C_3 bilayers. Six different types of bonded 2D B_4C_3 bilayers are found, classified by the bonding characteristics. The phonon spectrum calculations and ab initio molecular dynamics (AIMD) simulations demonstrate their dynamic and thermal stabilities. The low formation energies suggest the high possibility to realize them in experiments. Moreover, it is found that their Young's moduli are higher than that of the monolayer,[23] and the bonding characteristics enrich the electronic characteristics. Thus, our findings suggest the existence of bonded 2D B_4C_3 bilayer materials with unique properties.

2. COMPUTATION METHODS

All of the computations were performed by the Vienna ab initio simulation package (VASP) based on density functional theory (DFT).[24,25] The electron−ion interaction was described by the projector augmented wave (PAW) method,[26] and the exchange-correlation functional was adopted by the Perdew−Burke−Ernzerhof generalized gradient approximation (PBE-GGA) functional.[27] The cutoff plane-wave kinetic energy was set as 520 eV. The convergence of total energy for the self-consistent wave function and the force between atoms was set to 10^{-6} eV and 0.01 eV·Å^{-1}, respectively. To avoid the interaction between different layers, the vacuum thickness was set as 20 Å along the *c* direction. The Brillouin zone sampling was performed on Monkhorst−Pack meshes of 8 × 15 × 1 and 17 × 34 × 1 for structural optimization and electronic structure calculations, respectively. The vdW-DF functional[28] was adopted for the description of the van der Waals interactions. Additionally, the phonon spectrum calculations and ab initio molecular dynamics (AIMD) simulations were employed to estimate the dynamic and thermal stabilities at room temperature, respectively. The total simulation time was

https://doi.org/10.1021/acsomega.1c01073
ACS Omega 2021, 6, 13218−13224

set to 21 ps with steps of 3 fs in the NVT ensemble for AIMD simulations.

The formation energy (E_f) and cohesive energy (E_{coh}) were evaluated using the following formulas

$$E_f = \frac{E_t - m\mu_B - n\mu_C}{(m+n)} \quad (1)$$

$$E_{coh} = \frac{mE_B + nE_C - E_t}{(m+n)} \quad (2)$$

where μ_B and μ_C are the chemical potentials of the α-B-sheet[29] and graphene, respectively; E_t is the total energy; E_C and E_B represent the energy of a single C atom and a B atom, respectively; and n and m represent the number of C and B atoms.

The 2D Young's moduli (Y^{2D}) were evaluated using the following formulas[30]

$$Y_a^{2D} = \frac{c_{11}c_{22} - c_{12}c_{21}}{c_{22}} \quad (3)$$

$$Y_b^{2D} = \frac{c_{11}c_{22} - c_{12}c_{21}}{c_{11}} \quad (4)$$

where c_{xy} represents elastic constants; and a and b represent the direction of the crystal lattice, respectively.

3. RESULT AND DISCUSSION

3.1. Geometric Structure. We constructed many different bilayer structures based on the unique structural and electronic properties of the B_4C_3 monolayer.[21,22] Meanwhile, the stacking structures of two monolayers with distinct symmetries were considered. We constructed 25 bilayer structures, and after structural relaxations, we finally obtained six representative bonded bilayer structures (see Figure 1, labeled as I to VI, respectively) and nine vdW bilayer structures (see Figure S2). Since these bonded bilayer structures are much more energy favored than the vdW bilayer, we focus on the bonded bilayer structures. As shown in Figure 1, each unit cell contains 28 atoms in total (16 B and 12 C atoms). The bonded bilayer is different in the interface of the formed bond structures. It is worth mentioning that they look like the sandwiched B_4C_3 triple layer, with some inner B atoms acting as the sandwiched layer. Especially in B_4C_3-I, the inner B atom looks like an additional embedded atom, and some B−B bonding forms between them. Actually, we have not implanted any B or C atoms. At the beginning of the structural relaxation, each of them is a vdW bilayer system with different symmetries and stacking structures. Doubtlessly, atomic reorganizations have occurred due to the fact that the bonded bilayer is more favorable than the vdW bilayer in energy. Subsequently, the hybridization characteristics of some B atoms have changed, making them move out of the plane and presented as the inner atoms.

One can see that two types of B−B bonds are formed, the paralleled one with a bond length of 1.70 Å in B_4C_3-I and the vertical one with a bond length of 1.66 Å in B_4C_3-III. The bond length values are close to the reported B monolayer (1.71 and 1.70 Å),[29,31,32] suggesting that such bilayer structures are really chemical-bonded systems. In other types of bilayer structures, the two layers are connected together with B−C bonds. The B−C bond lengths are found in the range from 1.56 to 1.68 Å, which are close to the reported value in BC_3 (1.58 Å),[33] indicating a similar binding strength of the formed B−C covalent bond.

Interestingly, the inner B in B_4C_3-V is four-coordinated and the formed four B−C bond lengths are 1.68, 1.76, 1.76, and 1.75 Å. Generally, the bond length is consistent with the hybridization types. As for traditional sp^3 hybridization, the four bonds should have a similar bond length. Noted that the bond lengths for the four B−C bonds are very close to 1.7 Å, which indicates an sp^3 feature. For surface B, it adopts a three-coordinated sp^2 feature, and the formed three B−C bond lengths are 1.54, 1.54, and 1.58 Å, which is also consistent with the hybridization types. Apart from this, there are some other unexpected bonding features such as hexacoordinate B and planar tetracoordinate C found in this new family of 2D B_4C_3 systems.

The lattice constants, the thickness of the interlayer, the formation energy, and the cohesive energy of the six bilayer systems are summarized in Table 1. The calculated lattice constants a and b in the B_4C_3 monolayer are 8.08 and 4.66 Å, respectively.

Table 1. Predicted Lattice Constants (a and b), Cohesive Energy (E_{coh}), Formation Energy (E_f), and the Thickness of the Interlayer (d) of the Bonded B_4C_3 Bilayers

	a (Å)	b (Å)	E_{coh} (eV)	E_f (eV)	d (Å)
I	8.10	4.65	6.659	−0.055	3.93
II	8.05	4.66	6.682	−0.077	3.25
III	7.84	4.67	6.683	−0.078	3.26
IV	8.06	4.63	6.687	−0.083	4.50
V	8.06	4.63	6.683	−0.079	3.65
VI	8.01	4.68	6.676	−0.072	3.64

As shown in Table S3, the lattice constants of bonded B_4C_3 bilayers are smaller (<2.9%) than that of the monolayer, indicating the effects of atomic reorganizations on the lattice constants. Meanwhile, the atomic reorganization induces the thickness of the bilayer change in the range from 3.25 to 4.50 Å.

3.2. Stabilities. One can see in Table 1 that the lowest formation energy is found in B_4C_3-IV (−0.083 eV per atom), while the largest one is for B_4C_3-I (−0.055 eV per atom). Anyway, the formation energies of such bilayer systems are less than zero, indicating that they are energetically stable and are possible to be obtained in experiments. For comparison, we also calculated the formation energies of all of the considered bonded bilayers using the energies of boron in the most stable boron solid (Table S2), and the same conclusion is reached.

To evaluate the thermodynamic stability, we calculated the cohesive energy. Table 1 shows that the cohesive energy is about 6.659−6.687 eV per atom in this system. For comparisons, we calculated the cohesive energy and formation energy of the reported sandwich-like B_4C_3 triple layer,[20] B_4C_3 monolayer,[21,22] and homogeneous vdW B_4C_3 bilayer (see Figure S1). The obtained results are given in Table S1. One can see that the cohesive energies of our B_4C_3 bilayers are close to the reported B_4C_3 triple layer (6.707 eV) and are relatively higher than those of the two types of B_4C_3 monolayer structures (6.55 and 6.58 eV), suggesting the stability of our system. Interestingly, the binding strength of bonded bilayers is higher by 0.59−1.13% than that of the vdW bilayer. Such differences suggest that the bonded bilayers are much easier to be prepared than the vdW bilayer and the monolayer.

https://doi.org/10.1021/acsomega.1c01073
ACS Omega 2021, 6, 13218−13224

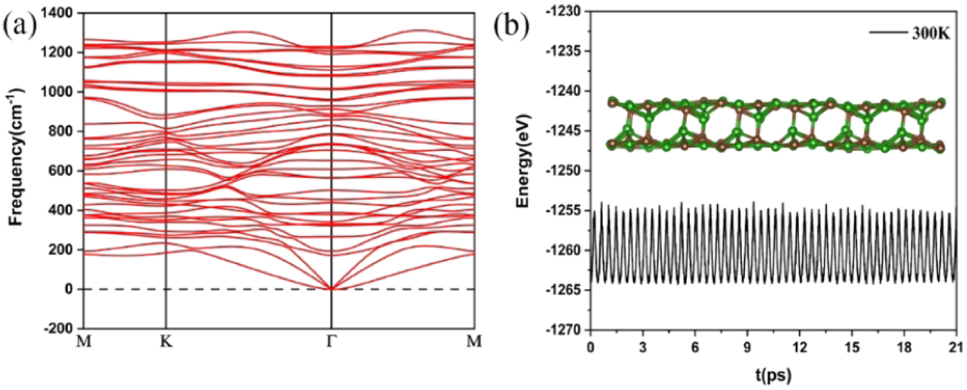

Figure 2. Calculated phonon band structure (a) and AIMD results (b) for B_4C_3-II, and the inset shows the snapshot of B_4C_3-II at 21 ps.

To further evaluate the dynamic and thermal stabilities of the new structures, we performed phonon spectrum calculations and AIMD simulations at 300 K, respectively. As an example, we have shown the phonon band structure and AIMD results of B_4C_3-II in Figure 2. One can see that there is no imaginary frequency (IF) for B_4C_3-II, and the bonded structure keeps very well after 21 ps MD simulations, suggesting that B_4C_3-II can really exist and the structure is stable at room temperature. For other systems, the results are given in Figures S2 and S3. Except for B_4C_3-I, all of the proposed structures are dynamically stable. Notably, the AIMD results demonstrated that such structures are stable at 300 K and thus suitable for applications at room temperature. Meanwhile, the highest frequency of B_4C_3-II reaches 1311 cm^{-1}, which is slightly lower than the frequency of BC_3 (1500 cm^{-1})[34] but much higher than that of B_2C (1167 cm^{-1}),[35] indicating that strong B−B and B−C bonds are formed in the bonded bilayer systems.

Interestingly, previous works have shown that in the B_4C_3 monolayer, the conduction band minimum (CBM) and the valence band maximum (VBM) are mainly contributed by the B and C atoms, respectively.[21] Our finding demonstrated that when two B_4C_3 monolayers are stacked together, the CBM of one layer can fit exactly with the VBM of the other layer. Electrons exchange between them and atomic recombinations occur naturally, giving rise to the formation of some bonds at the interface region and directly resulting in the bonded B_4C_3 bilayer with largely reduced energy (0.077−0.107 eV per atom).

3.3. Mechanical Properties. For mechanical stability and applications, we calculated the in-plane stiffness of each bonded bilayer system. There are five nonzero 2D elastic constants for the rectangle lattice, which are c_{11}, c_{22}, c_{66}, c_{12}, and c_{21} (using the standard Voigt notation: 1 − *xx*, 2 − *yy*, 6 − *xy*).[30] As listed in Table 2, the elastic constants of each bonded bilayer system meet the mechanical stability criterion,[36] i.e., $c_{11}c_{22} - c_{12}c_{21} > 0$ and $c_{66} > 0$. For the structures connected by B−C bonds, they possess relatively higher in-plane Young's moduli than those connected by B−B bonds. It is worth noting that the calculated values of the in-plane Young's moduli of B_4C_3-II (B_4C_3-V) along the *a*- and *b*-axes are 382(401) and 417(388) GPa·nm, respectively, which are higher than those of the B_4C_3 monolayer (356.8 GPa·nm)[22] and graphene (340 GPa·nm,[23] 338 GPa·nm from our calculations). It is well known that graphene is a very strong 2D material. This means that such bonded 2D B_4C_3 bilayers can be used as thin-layer materials, for instance, buffer layer protection materials in nanomechanics. Meanwhile, it should also be noted that Young's moduli for B_4C_3-III and B_4C_3-VI along the *a*-axis are around 100 GPa·nm smaller than those along the *b*-axis, indicating a strong anisotropic mechanical property. Such findings can enrich the growing anisotropic 2D materials.

Table 2. Calculated Elastic Constants (c_{ij}) and Young's Moduli (Y_a and Y_b) (Unit: GPa·nm)

	c_{11}	c_{22}	c_{66}	c_{12}	Y_a	Y_b
I	313	355	102	76	295	335
II	396	432	161	77	382	417
III	279	380	146	88	258	352
IV	340	383	181	63	329	371
V	415	402	178	74	401	388
VI	384	442	87	87	336	422

3.4. Electronic Properties. The electronic properties of each bilayer are calculated using the GGA-PBE method. The obtained band structures and PDOS are plotted in Figure 3. Interestingly, B_4C_3-I and B_4C_3-III exhibit metallic properties, while the others are semiconductors. One can see in Figure 3a,c that there exist three well-delocalized bands crossing the Fermi level. So many delocalized bands right at the Fermi level result in high DOS at the Fermi level,[37] demonstrating very high conductivity and thus great applications in nanoelectronics. This can be well understood by the fact that B_4C_3-I and B_4C_3-III contain B−B bonds at the interface region. It is noted that B tends to form a multicenter bond to share electrons. The formed B−B bonds are responsible for the high conductivity of such two bilayer types. It also suggests that creating some B−B bonds in other materials could be a perfect strategy to obtain high conductivity characteristics.

To further understand the high conductivity, in Figure S4, we have given out the partial charge distribution of the two bilayer systems in a small energy window near the Fermi level (blue region, as shown in Figure 3a,c). For B_4C_3-I, one can see that the charge densities are distributed among each of the sp^2-hybridized C atoms and the B−B dimer region. For B_4C_3-III, the charge densities are distributed among each C atom. It is known that B is a deficient atom, it tends to form a multicenter bond to share electrons. When the protruding B atom bonds with its adjacent B atoms, it changes the hybridization type of C atoms, which originally bond with the abovementioned sp^3- to sp^2-hybridized B atoms, releasing some p_z electrons, and accordingly improves the number of electronic states at the Fermi level. The increased delocalized bands right at the Fermi

https://doi.org/10.1021/acsomega.1c01073
ACS Omega 2021, 6, 13218−13224

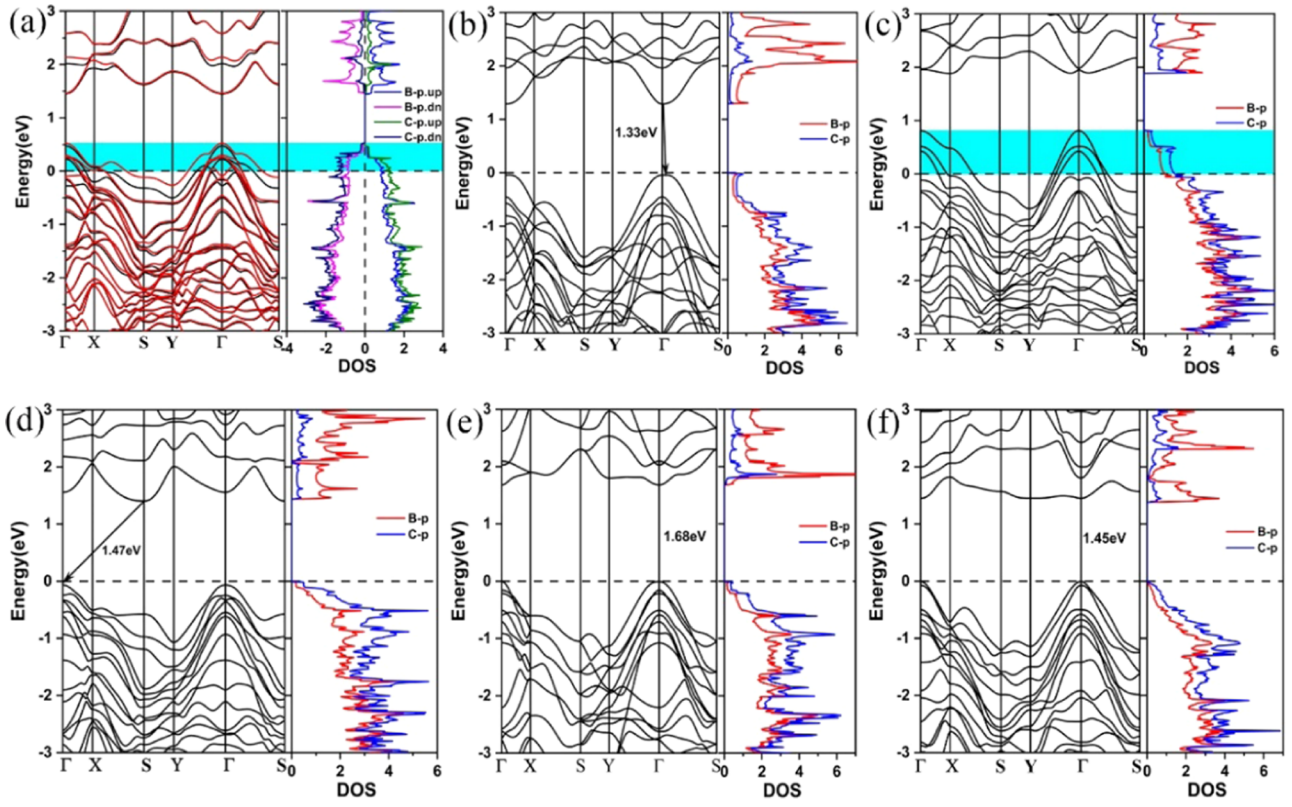

Figure 3. Calculated band structures and PDOS of (a) B_4C_3-I, (b) B_4C_3-II, (c) B_4C_3-III, (d) B_4C_3-IV, (e) B_4C_3-V, and (f) B_4C_3-VI. The black dashed line represents the Fermi level.

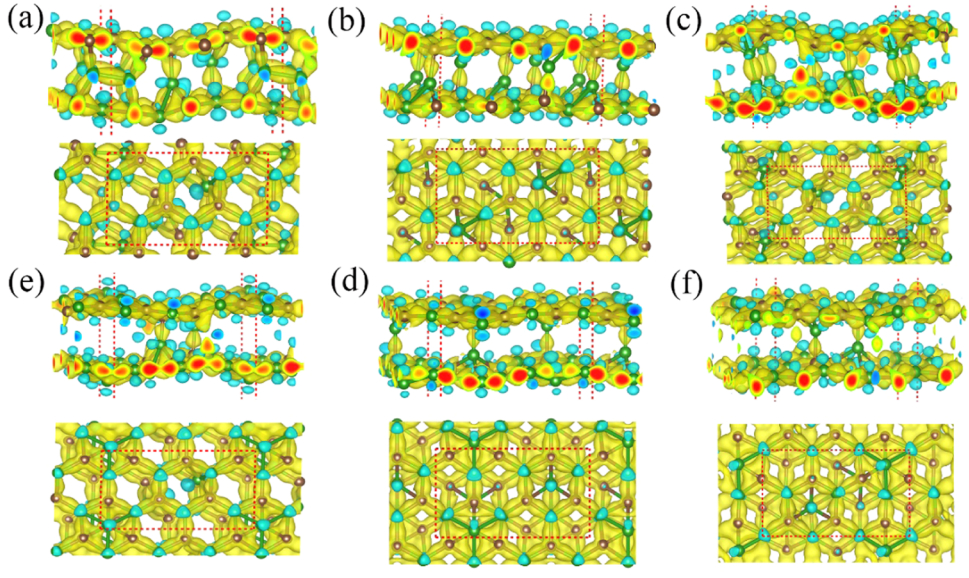

Figure 4. Calculated deformation charge distribution including the side view (upper) and top view (lower) of (a) B_4C_3-I, (b) B_4C_3-II, (c) B_4C_3-III, (d) B_4C_3-IV, (e) B_4C_3-V, and (f) B_4C_3-VI. The upper and down are the side view and top view, respectively. The isovalue is 0.13 eV $Å^{-3}$. Blue and yellow indicate charge reduction and accumulation, respectively.

level result in high DOS at the Fermi level, demonstrating the high conductivity. Additionally, B_4C_3-I exhibits a magnetic moment of 0.45 μ_B per unit cell, and the spin density is mainly located at the sp^2-hybridized C atoms and the B−B dimer region (see Figure S5), suggesting potential applications in spintronics.

For the other four types of bilayers, they are semiconductors with a band gap in the range from 1.33 to 1.68 eV, suggesting potential applications in photovoltaics. B_4C_3-V and B_4C_3-VI are direct band gap semiconductors, and B_4C_3-II and B_4C_3-IV are indirect band gap semiconductors. The main difference between B_4C_3-II and B_4C_3-IV is that the CBM and the VBM of B_4C_3-II are very close to the Γ position; thus, it is highly possible to turn into a direct band gap semiconductor. For each of them, the DOS shows clearly that the CBM and the

https://doi.org/10.1021/acsomega.1c01073
ACS Omega 2021, 6, 13218−13224

VBM are contributed by the coupled B $2p_z$ and C $2p_z$ electrons, inducing the π bond nature.

Our above analysis indicates that the formed bond structures at the interface play a decisive role in determining the stability and properties of such a system. To further understand the bond nature, we calculated the deformation charge density $\Delta\rho(r)$ using $\Delta\rho(r) = \rho(r) - \sum_{\mu}\rho_{atom}(r - R\mu)$, where $\rho(r)$ is the total charge density and $\sum_{\mu}\rho_{atom}(r - R\mu)$ stands for the superposition of independent atomic charge densities. The results are given in Figure 4. One can see that the charge around the B atom is reduced, while the charge around the C atom is accumulated. This is understandable by noting the different electronegativities of C and B atoms. Also, there is a large amount of charge accumulation between the B and C atoms in the B−C layer, indicating a strong B−C covalent bond in the plane. For the interlayer domain, charge accumulations are found between the B−B dimers in B_4C_3-I and B_4C_3-III, implying that a B−B covalent bond is formed exactly.

4. CONCLUSIONS

In summary, we predict the existence of bonded 2D B_4C_3 bilayers. The structures, stability, and electronic and mechanical properties are evaluated using the first-principles methods. The main findings are as follows (1) The bonded 2D B_4C_3 bilayer is a new type of 2D B_4C_3 structure. (2) Six types of bilayer systems featured by the bond structures at the interface region are found. (3) Stabilities are verified by phonon spectrum calculations and ab initio molecular dynamics simulations at room temperature. (4) Two types of bilayers (B_4C_3-I and B_4C_3-III) contain some B−B dimer structures, and they are metallic materials with high conductivity. The other types are semiconductors with a band gap suitable for photovoltaic applications. (5) B_4C_3-II and B_4C_3-V possess ultrastrong in-plane stiffness, which is more extensive than graphene. B_4C_3-III and B_4C_3-VI show a strong anisotropic mechanical property along with the axial directions. (6) The formed bonding structures at the interface region play a decisive role in determining the properties of such a system.

■ ASSOCIATED CONTENT

Supporting Information

The Supporting Information is available free of charge at https://pubs.acs.org/doi/10.1021/acsomega.1c01073.

Obtained lattice constants; cohesive energies; formation energies; phonon band structures; AIMD results; partial charge density distribution; and spin density charge distribution in related systems (PDF)

■ AUTHOR INFORMATION

Corresponding Authors

Xiao-Fei Li − *School of Optoelectronic Science and Engineering, University of Electronic Science and Technology of China, Chengdu, Sichuan 610054, China;* orcid.org/0000-0002-0851-3885; Email: xf.li@uestc.edu.cn

Xinrui Cao − *Collaborative Innovation Center for Optoelectronic Semiconductors and Efficient Devices, Department of Physics, Xiamen University, Xiamen 361005, China; Fujian Provincial Key Laboratory of Theoretical and Computational Chemistry, Xiamen University, Xiamen 361005, China;* orcid.org/0000-0002-2998-8863; Email: xinruicao@xmu.edu.cn

Authors

Jiacai Shen − *Collaborative Innovation Center for Optoelectronic Semiconductors and Efficient Devices, Department of Physics, Xiamen University, Xiamen 361005, China*

Feng Zheng − *Collaborative Innovation Center for Optoelectronic Semiconductors and Efficient Devices, Department of Physics, Xiamen University, Xiamen 361005, China*

Shaoxian Wang − *Shandong Key Laboratory of Medical Physics and Image Processing & Shandong Provincial Engineering and Technical Center of Light Manipulations, School of Physics and Electronics, Shandong Normal University, Jinan 250358, China*

Zi-Zhong Zhu − *Collaborative Innovation Center for Optoelectronic Semiconductors and Efficient Devices, Department of Physics, Xiamen University, Xiamen 361005, China;* orcid.org/0000-0001-5353-4418

Shunqing Wu − *Collaborative Innovation Center for Optoelectronic Semiconductors and Efficient Devices, Department of Physics, Xiamen University, Xiamen 361005, China;* orcid.org/0000-0002-2545-0054

Yi Luo − *Department of Theoretical Chemistry and Biology, School of Biotechnology, Royal Institute of Technology, S-106 91 Stockholm, Sweden*

Complete contact information is available at: https://pubs.acs.org/10.1021/acsomega.1c01073

Notes

The authors declare no competing financial interest.

■ ACKNOWLEDGMENTS

This work was supported by the National Natural Science Foundation of China (22073076 and 21703178) and the Fundamental Research Funds for the Central Universities of China (20720190052 and 20720190050). The Swedish National Infrastructure for Computing (SNIC) and Xiamen University's High-Performance Computing Center are acknowledged for the supercomputer resources.

■ REFERENCES

(1) Gao, F.; Klug, D. D.; Tse, J. S. Theoretical study of new superhard materials: B_4C_3. *J. Appl. Phys.* **2007**, *102*, No. 084431.

(2) Guo, X. J.; He, J. L.; Xu, B.; Liu, Z. Y.; Yu, D.; Tian, Y. J. First-principles investigation of dense B_4C_3. *J. Phys. Chem. C* **2007**, *111*, 13679−13683.

(3) Sateesh, B.; Reddy, A. S.; Sastry, G. N. Towards design of the smallest planar tetracoordinate carbon and boron systems. *J. Comput. Chem.* **2007**, *28*, 335−343.

(4) Cui, Z. H.; Contreras, M.; Ding, Y. H.; Merino, G. Planar tetracoordinate carbon versus planar tetracoordinate boron: the case of CB_4 and its cation. *J. Am. Chem. Soc.* **2011**, *133*, 13228−13231.

(5) Liu, C.; Tang, M.; Wang, H. The conversion among various B_4C clusters: a density functional theoretical study. *J. Phys. Chem. A* **2007**, *111*, 704−709.

(6) Zhang, C.; Zhang, S.; Wang, Q. Bonding-restricted structure search for novel 2D materials with dispersed C_2 dimers. *Sci. Rep.* **2016**, *6*, No. 29531.

(7) Yan, W. W.; Li, X. F.; Zhang, X. H.; Cao, X. R.; Deng, M. S. Family-dependent magnetism in atomic boron adsorbed armchair graphene nanoribbons. *J. Mater. Chem. C* **2019**, *7*, 6241−6245.

(8) Wang, Z. X.; Schleyer, P. R. Construction principles of "hyparenes": Families of molecules with planar pentacoordinate carbons. *Science* **2001**, *292*, 2465−2469.
(9) Wu, X.; Pei, Y.; Zeng, X. C. B_2C graphene, nanotubes, and nanoribbons. *Nano Lett.* **2009**, *9*, 1577−1582.
(10) Pei, Y.; Zeng, X. C. Probing the planar tetra-, penta-, and hexacoordinate carbon in carbon-boron mixed clusters. *J. Am. Chem. Soc.* **2008**, *130*, 2580−2592.
(11) Zhou, P.; Ma, Z. S.; Sun, L. Z. Coexistence of open and closed type nodal line topological semimetals in two dimensional B_2C. *J. Mater. Chem. C* **2018**, *6*, 1206−1214.
(12) Karamanis, P.; Otero, N.; Pouchan, C. Planar tetra-coordinate carbon resulting in enhanced third-order nonlinear optical response of metal-terminated graphene nanoribbons. *J. Mater. Chem. C* **2013**, *1*, 8223.
(13) Dai, J.; Li, Z. Y.; Yang, J. L.; Hou, J. G. A first-principles prediction of two-dimensional superconductivity in pristine B_2C single layers. *Nanoscale* **2012**, *4*, 3032−3035.
(14) Yanagisawa, H.; Tanaka, T.; Ishida, Y.; Matsue, M.; Rokuta, E.; Otani, S.; Oshima, C. Phonon dispersion curves of a BC_3 honeycomb epitaxial sheet. *Phys. Rev. Lett.* **2004**, *93*, No. 177003.
(15) Yanagisawa, H.; Ishida, Y.; Tanaka, T.; Ueno, A.; Otani, S.; Oshima, C. Metastable BC_3 honeycomb epitaxial sheets on the $NbB_2(0001)$ surface. *Surf. Sci.* **2006**, *600*, 4072−4076.
(16) Yanagisawa, H.; Tanaka, T.; Ishida, Y.; Rokuta, E.; Otani, S.; Oshima, C. Phonon dispersion curves of stable and metastable BC_3 honeycomb epitaxial sheets and their chemical bonding: Experiment and theory. *Phys. Rev. B* **2006**, *73*, No. 045412.
(17) Jafari, A.; Ghoranneviss, M.; Elahi, A. S. Growth and characterization of boron doped graphene by Hot Filament Chemical Vapor Deposition Technique (HFCVD). *J. Cryst. Growth* **2016**, *438*, 70−75.
(18) Caretti, I.; Gago, R.; Albella, J. M.; Jiménez, I. Boron carbides formed by coevaporation of B and C atoms: Vapor reactivity, B_xC_{1-x} composition, and bonding structure. *Phys. Rev. B* **2008**, *77*, No. 174109.
(19) Luo, X. Y.; Yang, J. H.; Liu, H. Y.; Wu, X. J.; Wang, Y. C.; Ma, Y. M.; Wei, S. H.; Gong, X. G.; Xiang, H. J. Predicting Two-Dimensional Boron-Carbon Compounds by the Global Optimization Method. *J. Am. Chem. Soc.* **2011**, *133*, 16285−16290.
(20) Fan, D.; Lu, S. H.; Guo, Y. D.; Hu, X. J. Two-dimensional stoichiometric boron carbides with unexpected chemical bonding and promising electronic properties. *J. Mater. Chem. C* **2018**, *6*, 1651−1658.
(21) Tian, X.; Xuan, X.; Yu, M.; Mu, Y.; Lu, H. G.; Zhang, Z.; Li, S. D. Predicting two-dimensional semiconducting boron carbides. *Nanoscale* **2019**, *11*, 11099−11106.
(22) Chang, H.; Tu, K. X.; Zhang, X.; Zhao, J. X.; Zhou, X. M.; Zhang, H. J. B_4C_3 Monolayer with Impressive Electronic, Optical, and Mechanical Properties: A Potential Metal-Free Photocatalyst for CO_2 Reduction under Visible Light. *J. Phys. Chem. C* **2019**, *123*, 25091−25101.
(23) Lee, C.; Wei, X.; Kysar, J. W.; Hone, J. Measurement of the elastic properties and intrinsic strength of monolayer graphene. *Science* **2008**, *321*, 385−388.
(24) Kresse, G.; Furthmuller, J. Efficient iterative schemes for ab initio total-energy calculations using a plane-wave basis set. *Phys. Rev. B* **1996**, *54*, 11169−11186.
(25) Kresse, G.; Furthmuller, J. Efficiency of ab-initio total energy calculations for metals and semiconductors using a plane-wave basis set. *Comput. Mater. Sci.* **1996**, *6*, 15−50.
(26) Kresse, G.; Joubert, D. From ultrasoft pseudopotentials to the projector augmented-wave method. *Phys. Rev. B* **1999**, *59*, 1758−1775.
(27) Perdew, J. P.; Burke, K.; Ernzerhof, M. Generalized gradient approximation made simple. *Phys. Rev. Lett.* **1996**, *77*, 3865−3868.
(28) Dion, M.; Rydberg, H.; Schroder, E.; Langreth, D. C.; Lundqvist, B. I. van der Waals density functional for general geometries. *Phys. Rev. Lett.* **2004**, *92*, No. 246401.
(29) Zhou, X. F.; Dong, X.; Oganov, A. R.; Zhu, Q.; Tian, Y. J.; Wang, H. T. Semimetallic Two-Dimensional Boron Allotrope with Massless Dirac Fermions. *Phys. Rev. Lett.* **2014**, *112*, No. 085502.
(30) Andrew, R. C.; Mapasha, R. E.; Ukpong, A. M.; Chetty, N. Mechanical properties of graphene and boronitrene. *Phys. Rev. B* **2012**, *85*, No. 125428.
(31) Wu, X.; Dai, J.; Zhao, Y.; Zhuo, Z.; Yang, J.; Zeng, X. C. Two-dimensional boron monolayer sheets. *ACS Nano* **2012**, *6*, 7443−7453.
(32) Liu, Y. X.; Dong, Y. J.; Tang, Z. Y.; Wang, X. F.; Wang, L.; Hou, T. J.; Lin, H. P.; Li, Y. Y. Stable and metallic borophene nanoribbons from first-principles calculations. *J. Mater. Chem. C* **2016**, *4*, 6380−6385.
(33) Popov, I. A.; Boldyrev, A. I. Deciphering Chemical Bonding in a BC_3 Honeycomb Epitaxial Sheet. *J. Phys. Chem. C* **2012**, *116*, 3147−3152.
(34) Zhang, H.; Liao, Y.; Yang, G.; Zhou, X. Theoretical Studies on the Electronic and Optical Properties of Honeycomb BC_3 monolayer: A Promising Candidate for Metal-free Photocatalysts. *ACS Omega* **2018**, *3*, 10517−10525.
(35) Li, F.; Tu, K.; Zhang, H.; Chen, Z. Flexible structural and electronic properties of a pentagonal B_2C monolayer via external strain: a computational investigation. *Phys. Chem. Chem. Phys.* **2015**, *17*, 24151−24156.
(36) Born, M.; Huang, K. *Dynamical Theory of Crystal Lattices*; Clarendon Press: Oxford, 1954; Vol. *xii*, p 429.
(37) Wirtz, L.; Rubio, A. In *Band Structure of Boron Doped Carbon Nanotubes*, AIP Conference Proceedings, 2003; pp 402−405.

https://doi.org/10.1021/acsomega.1c01073
ACS Omega 2021, 6, 13218−13224